LAWRENCE
LIVERMORE
NATIONAL
LABORATORY

UCRL-PROC-217426

Large-Stroke Self-Aligned Vertical Comb Drive Actuators for Adaptive Optics Applications

E. J. Carr, S. S. Olivier, O. Solgaard

November 30, 2005

Photonics West
San Jose, CA, United States
January 21, 2006 through January 26, 2006

Large-Stroke Self-Aligned Vertical Comb Drive Actuators for Adaptive Optics Applications

Emily Carr
Department of Electrical and Computer Engineering, University of California, Davis, Davis, CA 95616
Lawrence Livermore National Laboratory, Livermore, CA 94550

Scot Olivier
Lawrence Livermore National Laboratory, Livermore, CA 94550

Olav Solgaard
Department of Electrical Engineering, Stanford University, EL Ginzton Laboratory, Stanford, CA 94035

ABSTRACT

A high-stroke micro-actuator array was designed, modeled, fabricated and tested. Each pixel in the 4x4 array consists of a self-aligned vertical comb drive actuator. This micro-actuator array was designed to become the foundation of a micro-mirror array that will be used as a deformable mirror for adaptive optics applications. Analytical models combined with CoventorWare® simulations were used to design actuators that would move up to 10μm in piston motion with 100V applied. Devices were fabricated according to this design and testing of these devices demonstrated an actuator displacement of 1.4μm with 200V applied. Further investigation revealed that fabrication process inaccuracy led to significantly stiffer mechanical springs in the fabricated devices. The increased stiffness of the springs was shown to account for the reduced displacement of the actuators relative to the design.

Keywords: Adaptive optics, wavefront correction, micromechanical mirror device, piston-type mirror elements, spatial light modulator, surface micromachining, MOEMS

I. INTRODUCTION

Adaptive optics are used to correct for variable aberrations in optical systems. For instance, in astronomical imaging from ground-based telescopes, adaptive optics are used to correct for the aberrations introduced by the Earth's atmosphere. In other optical systems the aberrations that need to be corrected could be caused by optical fabrication errors, thermally induced distortions [1], or in the case of vision science, aberrations that are inherent in the human eye [2].

A deformable element is required in an adaptive optics system to "correct" the wavefront that has been distorted by these aberrations. Each adaptive optics (AO) application has its own set of requirements for this deformable element. In the case of a vision science AO system, the requirements can be seen in Table 1[3].

Table 1. Requirements for an adaptive optics deformable element to be used in a vision science application.

Number of Actuators	Actuator Range	Operating Frequency	Surface Quality	Fill Factor	Reflectivity visible, IR	Aperture
~200	~10 μm	> ~100 Hz	< ~20 nm	> ~97%	> ~ 80%	~ 10 mm

The ultimate goal of our work is to model, design, and fabricate a micromachined segmented deformable mirror using silicon technologies developed in IC fabrication to make large-stroke (10-15μm) micro-deformable mirrors for adaptive optics that can be used for vision science applications. Previous work has been done on high stroke micro-deformable mirrors using bulk micromachining [4-6], surface micromachining using bimorph actuators [7], magnetic actuation [8] and thermal actuation [9]. Our current goal is to use silicon micromachining processes with self-aligned vertical comb drives as our means of actuation for this project. It has been shown that large forces can be produced with this type of actuator, which allows a large vertical displacement to be realized with a low voltage applied [10]. This type of actuator has also been used to fabricate many different types of scanning micromirrors [11-19].

II. ACTUATOR ELECTROMECHANICAL MODELING AND SIMULATIONS

Vertical comb drive actuators are attractive because of the amount of force they generate relative to other designs. In previous work on micro-machined deformable mirrors, electrostatic parallel plate actuators have been used [20, 21]. The force on a parallel plate actuator is:

$$F_{pp} = \frac{\varepsilon_0 A_{pp} V^2}{2 d^2} \tag{1}$$

where ε_0 is the permittivity of free space (we assume the gap between plates is filled with air), A_{pp} is the plate area, V is the voltage applied between the plates, d is the initial gap. This type of actuator can be seen in Figure 1.

Figure 1. Schematic of a parallel plate actuator.

The electrostatic force of a vertical comb drive structure is:

$$F_{cd} = \frac{N \varepsilon_0 h V^2}{g} \tag{2}$$

where N is the number of comb pairs, ε_0 is the permittivity of free-space (again, we assume the gap between comb teeth is filled with air), h is the length of the comb teeth, V is the voltage applied the two sets of comb teeth, and g is the gap between the comb teeth. This type of actuator can be seen in Figure 2.

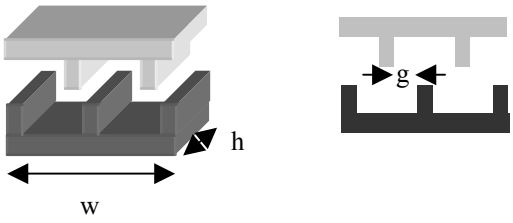

Figure 2. Schematic of a vertical comb drive actuator.

If we take the ratio of these two forces:

$$\frac{F_{cd}}{F_{pp}} = \frac{2 d^2 N h}{A_{pp} g} \tag{3}$$

we find, using a vertical comb drive structure that has been designed to have an area (wh) of $(885\mu m)^2$, that we are able to achieve $F_{cd} / F_{pp} = 21$, showing that combdrives are superior to parallel-plate actuators for this application.

Analytical Modeling: For this project, we are interested in the voltage versus displacement (z) characteristics of the vertical comb drive device. Using $F_{cd} = k_z z$, where k_z is the spring constant of the mechanical structure in the z-direction and z is the displacement, Equation (2) becomes:

$$z = \frac{N \varepsilon_o h V^2}{k_z g} \tag{4}$$

Studying Equation (4), we find that there are many factors that influence the displacement versus voltage characteristics of our device. N, h, and g are drawn features in our process masks. k_z is determined by the mechanical spring that we use. Balancing all of these factors, we decided that a folded spring would be the preferred design for a mechanical spring for our actuator. This type of spring is shown in Figure 3.

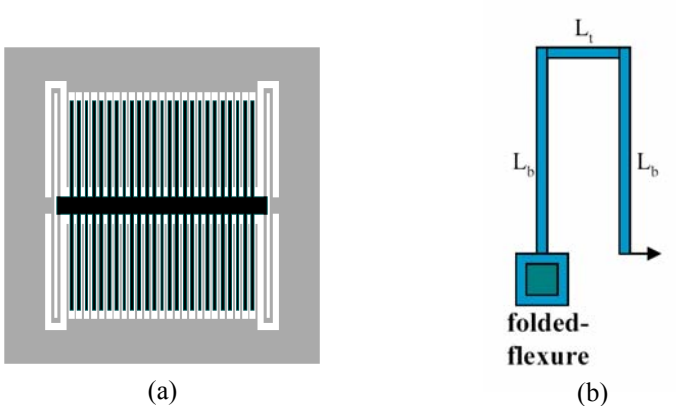

(a) (b)

Figure 3. (a) Model of one of our vertical comb drive devices with four folded-flexure springs. (b) Labeled folded spring schematic.

Folded Spring Design: For the folded spring (folded-flexure) design we are assuming that we have four fixed-guided folded beams that are acting as the mechanical springs. Any torsion or bending of the central beam, shown in Figure 3(a), has been neglected. The spring constant of one of the fixed-guided folded structures can be found using Equation 5. E is the Young's modulus of the material and $I_{x,b}=(w_b\ t_b^3)\ /\ 12$.

$$k_z = \frac{6EI_{x,b}}{L_b^3} \tag{5}$$

Taking into account that we have four cantilever beams, our effective spring constant for the folded spring design becomes:

$$k_z = \frac{2Ew_b t_b^3}{L_b^3} \tag{6}$$

Using Equation (6) in combination with Equation (4), we find the theoretical voltage vs. displacement curve for this type of spring with E=1.69×10^{11} Pascals, w_b=10.0×10^{-6}m, t_b=5.0×10^{-6}m, L_b=330×10^{-6}m, N = 50, h=comb overlap=length of effective comb=273×10^{-6}m, and g=6.0×10^{-6}m and ε_0 = 8.85×10^{12} F/m. The results are shown in Figure 4.

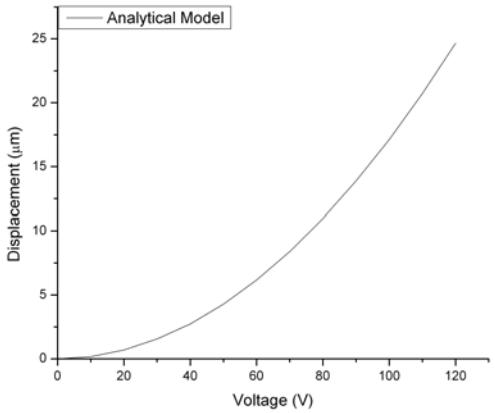

Figure 4. Voltage versus displacement curve for the folded-flexure design with N=50.

CoventorWare® Modeling: To complement our simple analytical models, we used a commercial 3-D multi-physics numerical analysis software package to verify our previous modeling results. The software that we chose was CoventorWare® modeling software. The 2-D representation of our actuator structure is found in Figure 3(a). The 3-D model is shown in Figure 5.

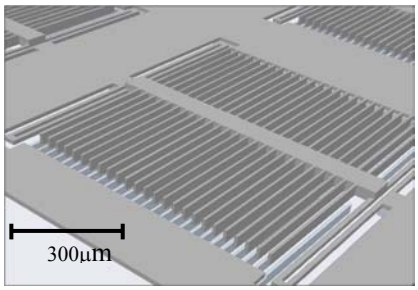

Figure 5. 3-D model of the folded spring structure that was modeled analytically.

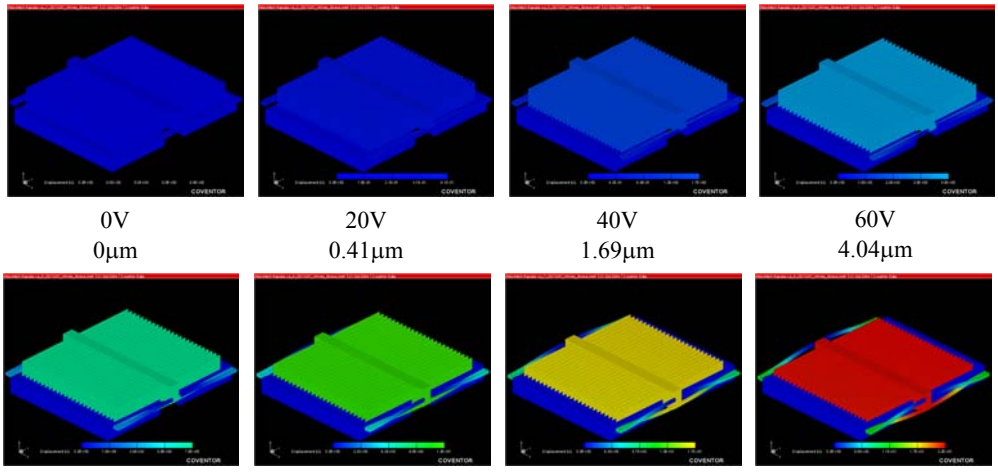

Figure 6. CoventorWare® modeling results of the folded-spring design.

The CoventorWare® software package enables schematic-based behavioral modeling. The 3-D representation of our model was drawn (as shown in Figure 5) and then boundary conditions, such as fixing the ends of the springs in the x,

y and z-directions, were put in place on the meshed model. Electro-mechanical modeling was then performed on the structure with a range of voltages. Results from this modeling can be found in Figure 6. The voltage vs. displacement results for the folded-flexure design using both the analytical spring model and the CoventorWare® electro-mechanical model are shown in Figure 7.

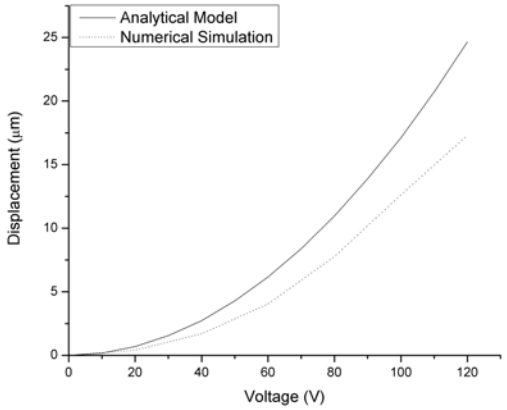

Figure 7. Voltage vs. displacement curve for both the analytical model of the folded-flexure design and the CoventorWare® modeling results.

III. FABRICATION

The fabrication process is shown in schematic form in Figure 8 (a)-(f). Figure 8(g) shows the line through which the cross-section in Figure 8 (a)-(f) are drawn. The process begins with a 4" silicon-on-insulator (SOI) wafer. The device layer is 25μm thick with a 2μm thick buried oxide layer. The first mask (Mask 1) contains the coarse comb teeth that

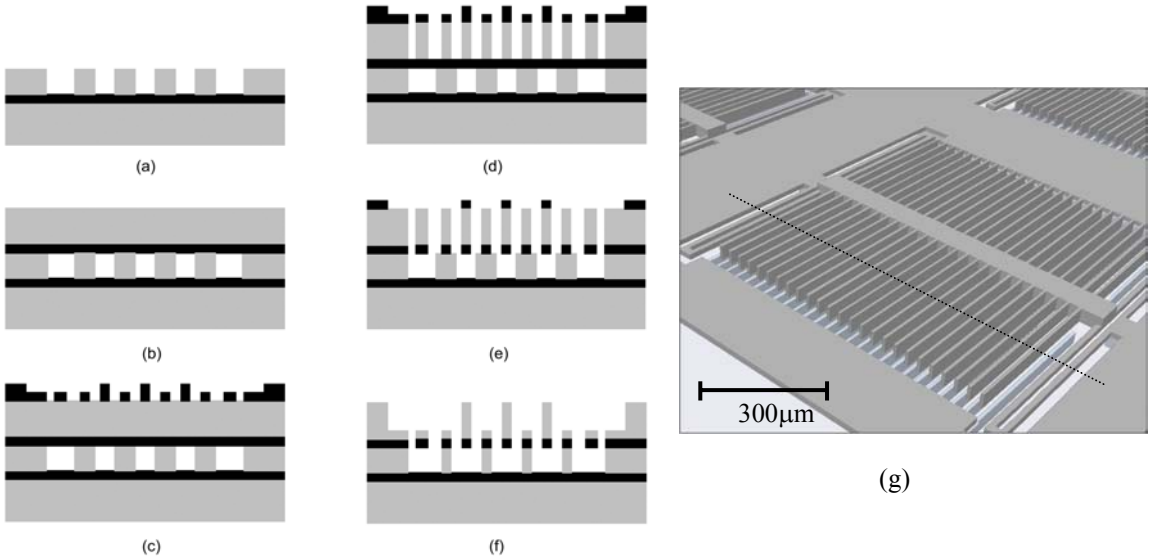

Figure 8. Schematic of the process flow for the large-stroke actuators. (a) SOI wafer that has had the top device layer etched to form the rough bottom comb teeth - DRIE. (b) Thermally oxidized wafer fusion bonded to the original wafer stack. (c) Two layer LTO mask formed using two masks. All of the combs are formed in this step – the self-aligned step. (d) The second device layer is etched in the DRIE etch through to oxide (e) The masking LTO is removed from above the rough combs and from above the springs (f) Etching continues with the DRIE forming the bottom combs and thinning the springs. This step is essential to achieve the voltage vs. displacement characteristics needed. (g) Line through which cross-section shows the process flow.

are shown in Figure 8 (a). This mask is etched using a STS DRIE through the full 25μm thick device layer. After this is complete, the wafer is cleaned using 3 H_2SO_4: 1 H_2O_2 for 10 minutes. A thermally oxidized wafer (0.5 μm thick) is then bonded to this SOI wafer and put in an oxidization furnace for ~ 2 hours. After this bonding is complete, a low-temperature oxide (LTO) is deposited to be used as an etch mask. The LTO is 1.5 μm thick. The next step (not shown in Figure 8) is to open alignment marks on the edge of the wafer so that our mask for the top comb teeth will align with the course comb teeth already etched. That is done with Align Mask A. After these areas are opened, Mask 2 is aligned. Mask 2 contains all of the comb teeth and the springs that are to be etched. Because all of the comb teeth are combined in the same mask, there is no critical alignment necessary. The alignment accuracy needed is $g/2$ [14]. After the 1.5 μm thick LTO has been etched fully using Mask 2, the mask is stripped and Mask 3 is applied. This mask covers the LTO that is over the top comb teeth. It allows the LTO that is above the bottom teeth and the springs to be thinned to ~0.5 μm thick. These two steps are combined in Figure 8 (c). The advantage we have in using LTO as our masking layer is that we do not have to define fine features on a wafer with deep topography. We are able to define our features with just the LTO patterned, which at 1.5μm thick is much thinner than the ~40μm thick top comb teeth. This dual-layer mask is very important to this process flow. In Figure 8 (d) we see the first DRIE etch using the dual layer mask shown in Figure 8 (c). The LTO masking oxide and the thermal oxide between the combs is then etched, as shown in Figure 8 (e). Then, the bottom combs are formed by another DRIE etch. The springs are also thinned during this process. This thinning is important for our design as it allows our device to achieve the large displacement with low voltages as shown in the modeling section above. After the fabrication was complete, testing was done to find the experimental voltage versus displacement relation for this actuator.

IV. EXPERIMENTAL RESULTS

The actuators shown schematically in Figure 8 were fabricated and tested. Figure 9 (a) and (b) show the actuators as seen in a Wyko white-light interferometric microscope as a potential difference was applied between the top and bottom comb teeth. Figure 9 (a) shows the actuator at its rest position, or 0V. A voltage of 100V is then applied to the bottom comb teeth with the top held at ground. The fringes move on the actuator itself but not on the stationary panel on the right side of the image, as shown in Figure 9 (b).

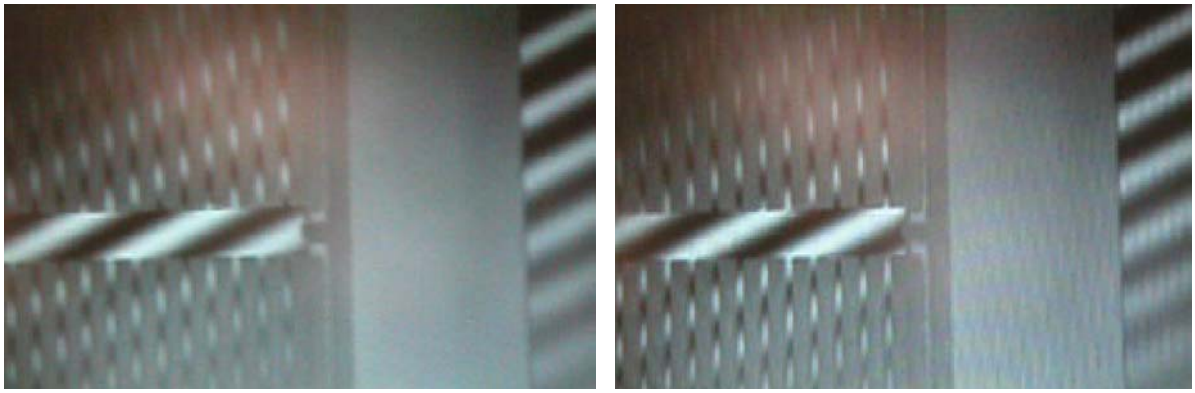

(a) (b)

Figure 9. (a) 0 V applied to the bottom comb teeth. Note fringes on right hand portion of picture. (b) 100V applied to the bottom comb teeth. Note that the fringes have moved on the actuator but have stayed the same on the right side of the picture. This shift implies movement of the actuator.

The next step was to quantify the movement of these actuators and compare them to the theoretical motion that was described in previous sections. Before this was done, we examined the fabricated structures using a SEM. The SEM pictures of the spring and the bottom and top comb teeth are found in Figure 10. We had found, using a Tencor surface profilometer, that the springs had not been thinned as much as we had originally designed them to be. In other words, t_b in Equation (6) was not 5μm as we had designed, but was instead 18 μm. We were able to verify this result with the SEM picture. So, our theoretical voltage vs. displacement also changed because our k_z value changed. We also had noted that the gap between the comb teeth also increased from a drawn 6 μm to 7 μm during processing. This measurement was done with a calibrated optical microscope. This was also confirmed with the SEM picture.

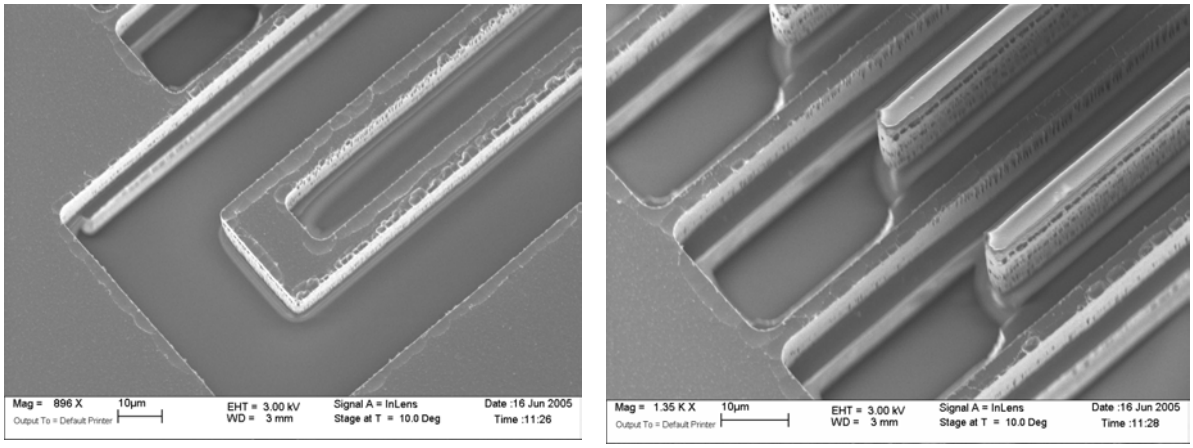

Figure 10. SEM pictures of fabricated folded-spring large-stroke actuators. (a) SEM of the spring itself. The thickness of this spring after fabrication is 18μm instead of the 5μm as originally designed. This thickness was measured using a Tencor surface profilometer on test structure designed to measure the thickness of this etched layer. (b) SEM of the top and bottom comb teeth. Note that the gap between comb teeth has increased from a drawn 6 μm to a measured 7 μm after fabrication. This was measured with a calibrated optical microscope.

An example of our displacement measurements is shown in Figure 11. The fabricated actuator had a potential difference applied between the top and bottom comb teeth. As each voltage was applied, data was collected from interferometric measurements. The displacements could be obtained by measuring the displacement of the actuator compared to the non-moving edge. An example of this is shown in Figure 11 (a). From these images, line scans were

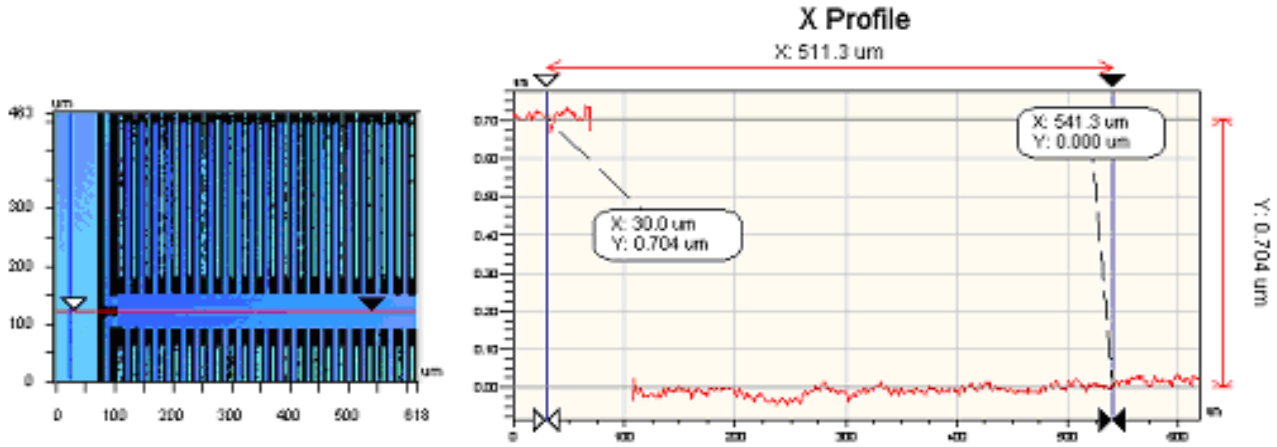

(a) (b)

Figure 11. Analysis of the displacement of a large-stroke actuator using the Wyko white-light interferometric microscope. (a) False color image of the displacement of the actuator. (b) X profile of the actuator showing the different in heights of the edge (not actuated) and the pulled down actuator (140V applied).

made through the stationary and moving portion of the actuator. An example of the results is shown in Figure 11(b), which demonstrates how the actuators move when a potential difference is applied between the comb teeth.

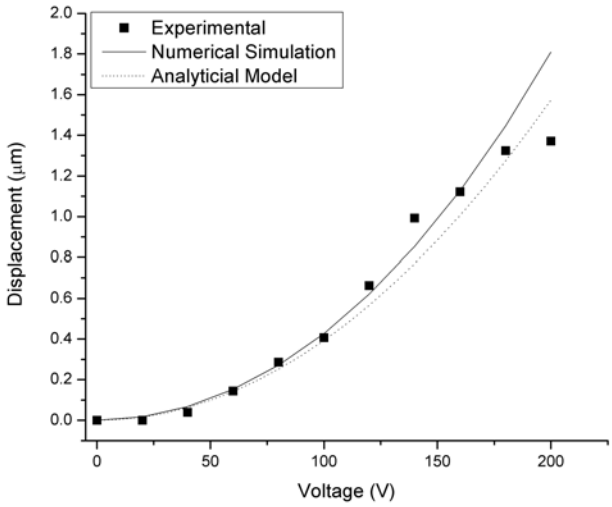

Figure 12. Voltage vs. displacement theory and experiment for fabricated folded-flexure device. The thickness of the spring has changed from 5μm to 18μm and the gap between the combs has changed from 6μm to 7μm.

Figure 12 shows the revised voltage versus displacement characteristics that are predicted, after taking into account the observed thickness increase of the spring structures, with both the analytical and the CoventorWare® model of the springs. Figure 12 also shows the experimental results from the data obtained from the Wyko interferometer. Comparison of the data and theory demonstrate that both models for our folded flexure spring agree well with our experimental voltage versus displacement data.

V. FUTURE WORK

These prototype actuators were designed to be the foundation for a micro-mirror array that would be used as a deformable mirror for adaptive optics applications. In order to accomplish this, it is necessary to bond another silicon wafer on top of the actuators. Additional processing is then required to release and segment the mirrors. In all, this becomes a six-mask process with four masks to make the mechanical-electrical-optical structures and two for aligning purposes. We also plan to modify the actuator fabrication process in order to produce thinner springs, as originally designed. This will allow us to achieve the 10μm stroke in a micro-actuator that is crucial for this application.

VI. CONCLUSION

A high-stroke micro-actuator array was designed, modeled, fabricated and tested. Each pixel in the 4x4 array consists of a self-aligned vertical comb drive actuator. This micro-actuator array is designed to be the foundation for an array of micro-mirrors to produce a deformable mirror for adaptive optics applications.. Analytical modeling of a folded spring actuator was performed as well as system modeling using CoventorWare® to determine the theoretical voltage versus displacement characteristics of this actuator. Both modeling techniques determined that the voltage versus displacement specifications for a large-stroke device suitable for vision science application would be met, 10μm of displacement for 100V applied between the vertical comb drive actuators. Using these models as a guide, a fabrication process was developed. As performed, the fabrication process resulted in springs that were thicker, and consequently stiffer, then originally planned. The fabricated springs allowed a displacement of 1.4μm when 200V was applied. Process development is ongoing to produce devices with thinner springs, in order to achieve the design displacement, and to attach mirrors to the actuator arrays.

This work was performed under the auspices of the U.S. Department of Energy by University of California, Lawrence Livermore National Laboratory under Contract W-7405-Eng-48.

REFERENCES

[1] R. K. Tyson, "Adaptive Optics Engineering Handbook." New York, NY: Marcel Dekker, Inc., 2000, pp. 339.

[2] J. Z. Liang, D. R. Williams, and D. T. Miller, "Supernormal vision and high-resolution retinal imaging through adaptive optics," *Journal of the Optical Society of America a-Optics Image Science and Vision*, pp. 2884-2892, 1997.

[3] P. Krulevitch, P. Bierden, T. Bifano, E. Carr, C. Dimas, H. Dyson, M. Helmbrecht, P. Kurczynski, R. Muller, S. Olivier, Y.-A. Peter, B. Sadoulet, O. Solgaard, and E. H. Yang, "MOEMS spatial light modulator development at the Center for Adaptive Optics," *MOEMS and Miniaturized Systems III*, vol. 4983, pp. 227-234, 2003.

[4] J. D. Mansell, P. B. Catrysse, E. K. Gustafson, and R. L. Byer, "Silicon deformable mirrors and CMOS-based wavefront sensors," presented at *High-Resolution Wavefront Control: Methods, Devices, and Applications II*, San Diego, CA, USA, 2000.

[5] L. M. Miller, M. L. Agronin, R. K. Bartman, W. J. Kaiser, T. W. Kenney, R. L. Norton, and E. C. Vote, "Fabrication and characterization of a micromachined deformable mirror for adaptive optics applications," presented at *Space Astronomical Telescopes and Instruments II,* Orlando, FL, USA, 1993.

[6] G. Vdovin, S. Middelhoek, and P. M. Sarro, "Technology and applications of micromachined silicon adaptive mirrors," *Optical Engineering*, vol. 36, pp. 1382-90, 1997.

[7] U. Srinivasan, M. A. Helmbrecht, C. Rembe, R. S. Muller, and R. T. Howe, "Fluidic self-assembly of micromirrors onto microactuators using capillary forces," *IEEE Journal of Selected Topics in Quantum Electronics*, vol. 8, pp. 4-11, 2002.

[8] O. Cugat, S. Basrour, C. Divoux, P. Mounaix, and G. Reyne, "Deformable magnetic mirror for adaptive optics: technological aspects," presented at *Proceedings IEEE Thirteenth Annual International Conference on Micro Electro Mechanical Systems*, Miyazaki, Japan, 2000.

[9] A. Tuantranont, L. A. Liew, V. M. Bright, Z. Wenge, and Y. C. Lee, "Phase-only micromirror array fabricated by standard CMOS process," *Elsevier. Sensors & Actuators A Physical*, pp. 1-2, 2001.

[10] S. Y. He and R. Ben Mrad, "Large-stroke microelectrostatic actuators for vertical translation of micromirrors used in adaptive optics," *IEEE Transactions on Industrial Electronics*, vol. 52, pp. 974-983, 2005.

[11] M. Fujino, P. R. Patterson, H. Nguyen, W. Piyawattanametha, and M. C. Wu, "Monolithically cascaded micromirror pair driven by angular vertical combs for two-axis scanning," *IEEE Journal of Selected Topics in Quantum Electronics*, vol. 10, pp. 492-497, 2004.

[12] D. Hah, C. A. Choi, C. K. Kim, and C. H. Jun, "A self-aligned vertical comb-drive actuator on an SOI wafer for a 2D scanning micromirror," *Journal of Micromechanics and Microengineering*, vol. 14, pp. 1148-1156, 2004.

[13] K. H. Jeong and L. P. Lee, "A novel microfabrication of a self-aligned vertical comb drive on a single SOI wafer for optical MEMS applications," *Journal of Micromechanics and Microengineering*, vol. 15, pp. 277-281, 2005.

[14] U. Krishnamoorthy, D. Lee, and O. Solgaard, "Self-aligned vertical electrostatic combdrives for micromirror actuation," *Journal of Microelectromechanical Systems*, vol. 12, pp. 458-464, 2003.

[15] S. Kwon, V. Milanovic, and L. P. Lee, "Vertical combdrive based 2-D gimbaled micromirrors with large static rotation by backside island isolation," *IEEE Journal of Selected Topics in Quantum Electronics*, vol. 10, pp. 498-504, 2004.

[16] D. Lee, U. Krishnamoorthy, K. Yu, and O. Solgaard, "Single-crystalline silicon micromirrors actuated by self-aligned vertical electrostatic combdrives with piston-motion and rotation capability," *Sensors and Actuators A-Physical*, vol. 114, pp. 423-428, 2004.

[17] V. Milanovic, G. A. Matus, and D. T. McCormick, "Gimbal-less monolithic silicon actuators for tip-tilt-piston micromirror applications," *IEEE Journal of Selected Topics in Quantum Electronics*, vol. 10, pp. 462-471, 2004.

[18] Q. X. Zhang, A. Q. Liu, J. Li, and A. B. Yu, "Fabrication technique for microelectromechanical systems vertical comb-drive actuators on a monolithic silicon substrate," *Journal of Vacuum Science & Technology B*, vol. 23, pp. 32-41, 2005.

[19] C. Tsou, W. T. Lin, C. C. Fan, and B. C. S. Chou, "A novel self-aligned vertical electrostatic combdrives actuator for scanning micromirrors," *Journal of Micromechanics and Microengineering*, vol. 15, pp. 855-860, 2005.

[20] M. A. Michalicek and V. M. Bright, "Flip-chip fabrication of advanced micromirror arrays," *Sensors and Actuators A Physical*, vol. 95, pp. 152-167, 2002.

[21] J. A. Perreault, T. G. Bifano, B. M. Levine, and M. N. Horenstein, "Adaptive optic correction using microelectromechanical deformable mirrors," *Optical Engineering*, vol. 41, pp. 561-566, 2002.